Available online at www.sciencedirect.com
ScienceDirect
Solid State Sciences 11 (2009) 233–239
Solid State Sciences
www.elsevier.com/locate/ssscie

Fe-doped SnO_2 transparent semi-conducting thin films deposited by spray pyrolysis technique: Thermoelectric and p-type conductivity properties

M.-M. Bagheri-Mohagheghi [a,b], N. Shahtahmasebi [a], M.R. Alinejad [a], A. Youssefi [c], M. Shokooh-Saremi [d,e,*]

[a] Nanotechnology Research Center, Department of Physics, Faculty of Basic Sciences, Ferdowsi University of Mashhad, Mashhad, Iran
[b] Department of Physics, Damghan University of Basic Sciences, Damghan, Iran
[c] Par-e-Tavoos Research Institute, Nanotechnology Laboratory, Mashhad, Iran
[d] Department of Electrical and Computer Engineering, University of Connecticut, Storrs, CT 06269-2157, USA
[e] School of Electrical Engineering and Robotics, Shahrood University of Technology, Shahrood, Iran

Received 9 January 2008; received in revised form 5 May 2008; accepted 7 May 2008
Available online 28 May 2008

Abstract

In this paper, we report structural, electrical, optical, and especially thermoelectrical characterization of iron (Fe) doped tin oxide films, which have been deposited by spray pyrolysis technique. The doping level has changed from 0 to 10 wt% in solution ([Fe]/[Sn] = 0–40 at% in solution). The thermoelectric response versus temperature difference has exhibited a nonlinear behavior, and the Seebeck coefficient has been calculated from its slope in temperature range of 300–500 K. The Hall effect and thermoelectric measurements have shown p-type conductivity in SnO_2:Fe films with [Fe]/[Sn] $\geq$ 7.8 at%. In doping levels lower than 7.8 at%, SnO_2:Fe films have been n-type with a negative thermoelectric coefficient. The Seebeck coefficient for SnO_2:Fe films with 7.8 at% doping level has been obtained to be as high as +1850 μV/K. The analysis of as-deposited samples with thicknesses ~350 nm by X-ray diffraction (XRD) and scanning electron microscopy (SEM) has shown polycrystalline structure with clear characteristic peak of SnO_2 cassiterite phase in all films. The optical transparency (T%) of SnO_2:Fe films in visible spectra decreases from 90% to 75% and electrical resistivity (ρ) increases from 1.2×10^{-2} to 3×10^{3} Ω cm for Fe-doping in the range 0–40 at%.

PACS: 73.61.Cw; 61.10.Kw; 68.37.Hk

Keywords: Tin oxide; Thermoelectric power; p-Type conductivity; Iron (Fe) doping; Spray pyrolysis

1. Introduction

Thermoelectric energy conversion, which directly transforms the heat into electricity, has drawn much attention in recent years and found applications in a variety of areas such as renewable and clean energy, thermoelectric power generation, small scale cooling systems for electronic devices, micro-refrigerator devices, and micro-thermo-chemistry on a chip for microelectronic components [1–3].

Seebeck (thermoelectric) coefficient (S) represents the rate of the voltage variation per unit temperature change ($\Delta V/\Delta T$) for the materials. This coefficient is very low for metals (only a few μV/K) and much larger for semiconductors (typically a few 100 μV/K). The aptitude of a material for thermoelectric applications is determined by using a dimensionless figure of merit $ZT = (S^2\sigma/\lambda)T$, in which S, σ, T and λ are, respectively, Seebeck coefficient, electrical conductivity, operating temperature and total thermal conductivity [4,5].

The thermoelectric materials are usually in the form of bulk, thin film and low-dimensional structures such as skutterudite-type ($CoAs_3$-type) alloys, clathrates (with general formula of $X_2Y_6E_{46}$, X and Y are guest atoms and E represents the Si, Ge, or Sn elements), Half-Heusler alloys such as MgAgAs

* Corresponding author. Department of Electrical and Computer Engineering, University of Connecticut, 371 Fairfield Road, U-2157, Storrs, CT 06269-2157, USA. Fax: +1 860 486 2447.
E-mail addresses: bmohagheghi@dubs.ac.ir (M.-M. Bagheri-Mohagheghi), saremi@engr.uconn.edu, mssaremi@yahoo.com (M. Shokooh-Saremi).

1293-2558/$ - see front matter © 2008 Elsevier Masson SAS. All rights reserved.
doi:10.1016/j.solidstatesciences.2008.05.005

(space group F3m), half-stuffed GaAs crystal structure, β-Zn_4Sb_3 alloys, chalcogenides such as Bi_2Te_3, PbTe and $CsBi_4Te_6$, complex oxides such as Na_xCoO_2, heavily doped n-type $SrTiO_3$, and thin films such as $Bi_{1-x}Sb_x$, Bi_2S_3, Na_x-CoO_2,
$Ca_3Co_4O_9$ alloys, and IV–VI nano-layers [1,5–11].

Since thin films are expected to have lower thermal conductivity than the bulk materials, due to strong phonon scattering at their interfaces, thermoelectric films likely open up the possibility for improvement of thermoelectric efficiency [9]. Although some thermoelectric materials, such as Bi_2S_3 and Bi_2Te_3 films, have found particular applications, their efficiencies at the best (ZT ∼ 1.0) are not enough for wider utilization in commercial applications. Thus, development of materials with high thermoelectric efficiencies is one of the main current research interests [9,12–16].

Tin oxide (SnO_2) thin film is well known as a wide band gap n-type semiconductor ($E_g = 3.6$–3.8 eV) with high simultaneous electrical conductivity and optical transparency in visible region of the spectrum [17]. So far, there are only a few reports on thermoelectric properties of SnO_2 thin films [18,19].

In this paper, we report preparation of p-type Fe-doped SnO_2 thin films with a large thermoelectric efficiency. The thermoelectrical, electrical, optical and structural properties of these films are studied using Seebeck and Hall effect measurements, X-ray diffraction, scanning electron microcopy (SEM) analysis, and UV–Vis absorption spectroscopy.

2. Experimental procedure

2.1. Deposition of SnO_2:Fe films by spray pyrolysis technique

The Fe-doped SnO_2 thin films have been deposited on glass substrates using a typical spray pyrolysis coating system [20]. The precursor solution was prepared by dissolving a certain amount (0.01 M) of stannic chloride ($SnCl_4{:}5H_2O$) and different amounts of iron chloride 6-hydrate ($FeCl_3{:}6H_2O$) in 10 ml of solvent (a mixture of double distilled water and ethanol in a volume ratio of 1:1). To enhance the solubility of stannic chloride, a few drops of HCl was also added to the solution [17,20]. The weight percentage (wt%) of $FeCl_3{:}6H_2O$ in solution was changed from 0 to 10 wt% (or atomic ratio of [Fe]/[Sn] = 0–40 at%). Before preparation of films, glass substrates were cleaned and placed on the hot plate and the undoped and Fe-doped SnO_2 films were deposited on rotating hot substrates with the conditions mentioned in Table 1. To prevent rapid reduction in the hot plate temperature, spraying is done in short time intervals. All experiments were done under approximately similar conditions.

2.2. Electrical and thermoelectrical measurements

For measuring the electrical resistivity and the thermoelectric electro-motive force (e.m.f.) of the films, two ends of samples were coated with aluminum by thermal evaporation in vacuum using Edwards E-306 coating system. In order to determine the concentration and type of majority carriers, Hall effect experiment was performed. By applying a constant longitudinal voltage ($V = 16.5$ V) and constant vertical magnetic field to the films ($B = 120$ mT), Hall transverse voltage (V_H) was measured. In this experiment, the effect of background (drift) voltage in absence of magnetic field was taken into account and compensated. Majority carrier concentration ($N_{n,p}$) was obtained using Eq. (1):

$$N_{n,p} = IB/|q|V_H t \tag{1}$$

In this equation, B, I, t, q and V_H are the magnetic flux density, measured current, film thickness, electron charge and Hall voltage, respectively. The sign of Hall voltage determines the type of majority carriers, (+) for the holes and (−) for the electrons.

The thermoelectric e.m.f. of the Fe-doped SnO_2 films was measured whilst applying a temperature gradient between the two ends of the samples at temperature range of 300–500 K [4]. An electric heater with electric power of 300 W for heating one side (hot-side) and an ice-water bath for cooling the other side (cold-side) were utilized. The Seebeck coefficients were determined by calculating the slope of the thermoelectric e.m.f. versus temperature difference between the hot and the cold ends of the samples.

Table 1
Spray deposition parameters for preparation of SnO_2:Fe films

Spray solution volume (ml)	10
Carrier-gas pressure (N_2) (atm)	3
Spray deposition rate (ml/min)	10
Nozzle to substrate distance (cm)	40
Spray nozzle diameter (atomizer) (mm)	0.2
Hot plate rotation speed (rpm)	60
Substrate temperature (°C)	500

2.3. Structural and optical characterization of films

X-ray diffraction (XRD) patterns of undoped and Fe-doped SnO_2 films were recorded by D8 Advance Bruker system using Cu Kα ($\lambda = 0.154056$ nm) radiation with 2θ in the range 20–70°. The average crystalline grain size was calculated using the Scherrer's formula based on the XRD patterns:

$$D = K\lambda/(\delta w \cos\theta) \tag{2}$$

where D is the average crystalline (grain) size, K is a constant (∼1), λ is the X-ray wavelength, δw is the full width at half maximum (FWHM) of XRD peaks and θ is the Bragg angle.

The surface morphology of films was studied by scanning electron microscopy (SEM) using LEO 1450 VP System. The optical absorption and transparency studies were performed in the wavelength range of 190–1100 nm using Agilent 8453 UV–Vis single beam spectrophotometer. The thickness of the films (t) was determined by using the optical transmission spectra (T%) and the following equation:

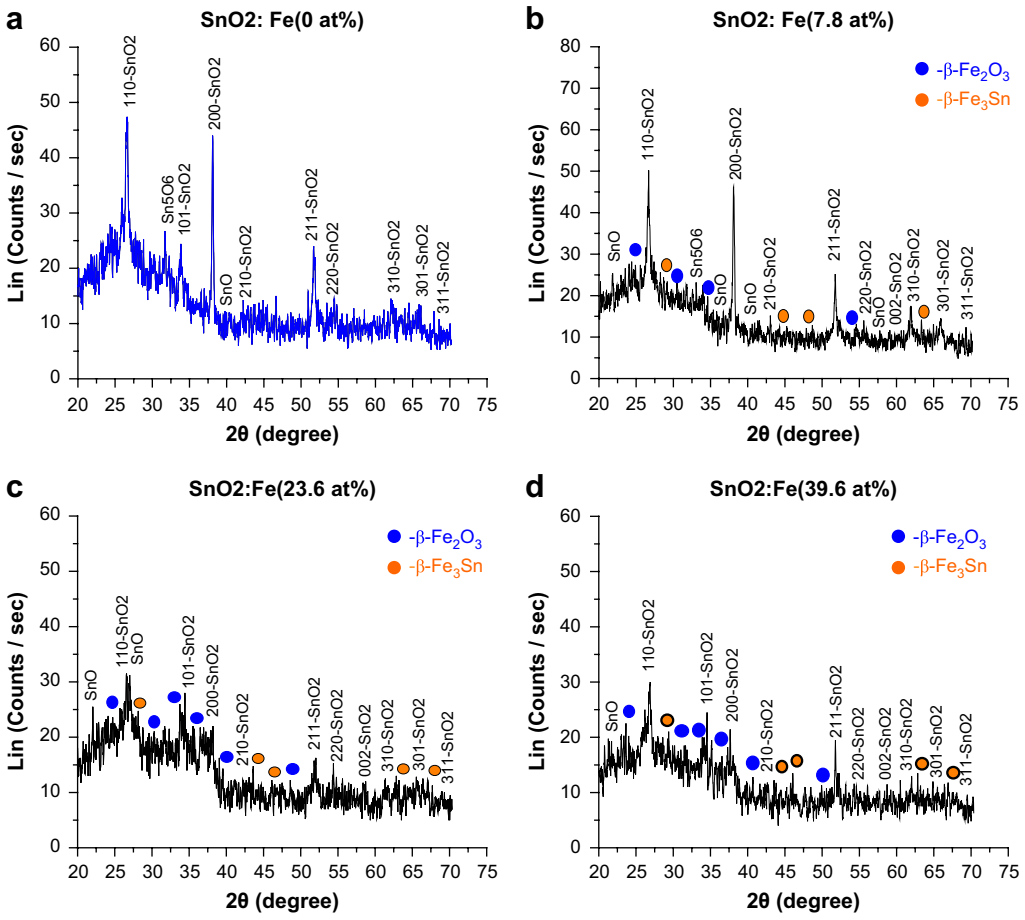

Fig. 1. X-Ray diffraction patterns of various Fe-doped SnO_2 films: (a) undoped SnO_2 film, (b) SnO_2:Fe (7.8 at%), (c) SnO_2:Fe (23.6 at%), and (d) SnO_2:Fe (39.6 at%).

$$t = \lambda_1\lambda_2/2n(\lambda_1 - \lambda_2) \tag{3}$$

in which, λ_1 and λ_2 are the two consecutive peaks in transmission spectra and n is the refractive index of SnO_2 ($n \sim 2$). The thickness of films was $\sim$350 nm in average.

The direct optical band gap (E_g) for various Fe-doping levels was obtained by optical absorption measurements and plotting $(\alpha h\nu)^2$ versus photon energy ($h\nu$) and using the following relation:

$$(\alpha h\nu)^2 = A(h\nu - E_g) \tag{4}$$

where α is the absorption coefficient, A and E_g are the constant and direct band gap of the material, respectively.

3. Results and discussion

3.1. Structural and electrical properties

Fig. 1(a)–(d) shows X-ray diffraction of deposited SnO_2:Fe films with doping levels from 0 at% to 40 at% in solution. As seem in Fig. 1(a)–(d) and Table 3, all SnO_2:Fe films with different doping levels have polycrystalline SnO_2

Table 2
The electrical and thermoelectrical measurement results of the SnO_2:Fe films for various dopant concentration (layer thicknesses are approximately equal to 350 nm)

Film + dopant (wt% in solution)	[Fe]/[Sn] (at% in solution)	Resistivity (ρ) (Ω cm)	Carrier concentration (cm^{-3})	Conductivity type	Seebeck coefficient (μV/K) $T = 350$ K	E_g (eV)
Undoped SnO_2	0	1.3×10^{-2}	-2.9×10^{19}	n	−255	3.87
SnO_2:Fe (1 wt%)	4	3.7×10^{-1}	-3.3×10^{18}	n	−287	3.83
SnO_2:Fe (2 wt%)	7.8	3.5×10^{2}	$+2.1 \times 10^{15}$	p	+1850	3.81
SnO_2:Fe (4 wt%)	15.7	63	$+1.2 \times 10^{16}$	p	+252	3.70
SnO_2:Fe (6 wt%)	23.6	70	$+4.0 \times 10^{15}$	p	+172	3.67
SnO_2:Fe (8 wt%)	31.5	1.05×10^{2}	$+2.2 \times 10^{15}$	p	+62.5	3.60
SnO_2:Fe (10 wt%)	39.6	3.36×10^{3}	$+1.8 \times 10^{15}$	p	+355	3.58

Table 3
Summary of the XRD parameters and mean grain size for different crystallographic orientations and various Fe concentrations

hkl	2θ (°)	Lattice distance (*d*) (Å)	Intensity (cP)	FWHM (°)	Mean grain size (nm)	Identification with (*hkl*) value
(a) Undoped SnO_2						
110	26.604	3.34	47.2	0.328	27.6	Tetragonal-SnO_2
101	33.879	2.64	25	0.247	37.4	Tetragonal-SnO_2
200	38.119	2.35	46	0.191	48.9	Tetragonal-SnO_2
211	51.7	1.76	24.5	0.267	36.8	Tetragonal-SnO_2
(b) SnO_2:Fe (7.8 at%)						
110	26.671	3.34	51.2	0.238	38.1	Tetragonal-SnO_2
101	33.98	2.63	24.5	0.152	60.7	Tetragonal-SnO_2
200	38.104	2.36	47.3	0.241	38.7	Tetragonal-SnO_2
211	51.769	1.76	26.7	0.181	54.3	Tetragonal-SnO_2
(c) SnO_2:Fe (23.6 at%)						
110	26.586	3.35	31.7	0.512	17.7	Tetragonal-SnO_2
101	34.429	2.60	27.2	0.425	21.7	Tetragonal-SnO_2
200	37.92	2.37	22	0.224	41.7	Tetragonal-SnO_2
211	52.019	1.75	16.6	0.204	48.2	Tetragonal-SnO_2
(d) SnO_2:Fe (39.6 at%)						
110	26.9	3.31	27.4	0.67	13.5	Tetragonal-SnO_2
101	34.54	2.59	24.1	0.329	28.1	Tetragonal-SnO_2
200	37.643	2.38	22.4	0.116	80.4	Tetragonal-SnO_2
211	51.772	1.76	18.4	0.115	85.4	Tetragonal-SnO_2

(with tetragonal-cassiterite phase) and SnO phases. However, by increasing doping level from 7.8 at% to 39.6 at%, other phases like β-Fe_2O_3 and β-Fe_3Sn appear. Also, in doping levels less than 23.6 at%, XRD peaks are stronger and amorphous background is weaker. Increasing the doping level, raises the amorphous phase, reduces the peak intensities and increases their width, which results in mean grain size reduction. Regarding atomic radius of Sn^{4+} (0.71 Å) and Fe^{3+} (0.64 Å), in lower doping levels, substitution of Fe^{3+} ions in network positions of Sn^{4+} is possible and clearly evident. Referring to Fig. 2, for up to 7.8 at% doping, the mean grain size at crystalline orientations of (110), (101) and (211) increases, and then for higher Fe concentrations decreases, which is related to formation of new phases such as β-Fe_2O_3 and β-Fe_3Sn.

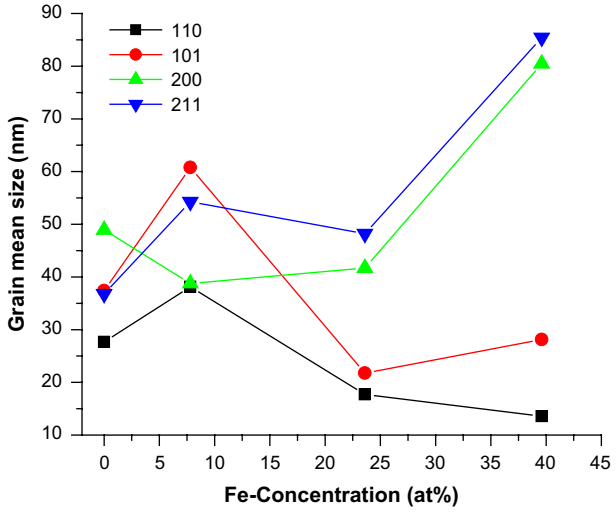

Fig. 2. The variations of mean grain size with various Fe concentration in crystalline orientations of (110), (101), (200) and (211).

Scanning electron microscopy (SEM) microstructural analysis (Fig. 3(a)–(d)) shows that with increasing the dopant level (>7.8 at%), grain size becomes smaller, in good agreement to the XRD pattern analysis. The SEM images also show a reduction of grain size from 60–80 nm (for undoped films) down to 25–45 nm in 23.6 at% doping level.

The results of the electrical and thermoelectrical measurements for Fe-doped SnO_2 films have been summarized in Table 2. The electrical measurements show that the electrical resistivity (ρ) of the films increases with increasing Fe-doping up to 7.8 at% and then decreases for doping up to 23.6 at%. The resistivity increases again in doping levels higher than 23.6 at%. The Hall effect experiment results also confirm that below 7.8 at% doping level the majority carriers are electrons (n-type conduction) and above this level are holes (p-type conduction). Also, referring to Seebeck coefficient values (*S*) at 350 K (Table 2), for doping levels less than 7.8 at%, the Seebeck coefficients of films are negative and for above this level are positive. These results exhibit a good agreement with Hall effect measurements. Indeed, compensation of electron for holes by increasing doping level up to 7.8 at% results in reduction of overall carrier concentration level. At 15.7 at% doping level, the concentration of majority carriers (now holes) is maximum (in order of 10^{16} cm^{-3}). By further increasing the acceptor dopant level, hole concentration decreases because of building up of structural disorders and the carrier traps.

3.2. Thermoelectrical properties

Fig. 4 illustrates the dependence of Seebeck coefficient to the temperature in the 300–500 K range. Variation of Seebeck coefficient at low temperatures is slow and nearly linear, which increases very fast with a nonlinear behavior with

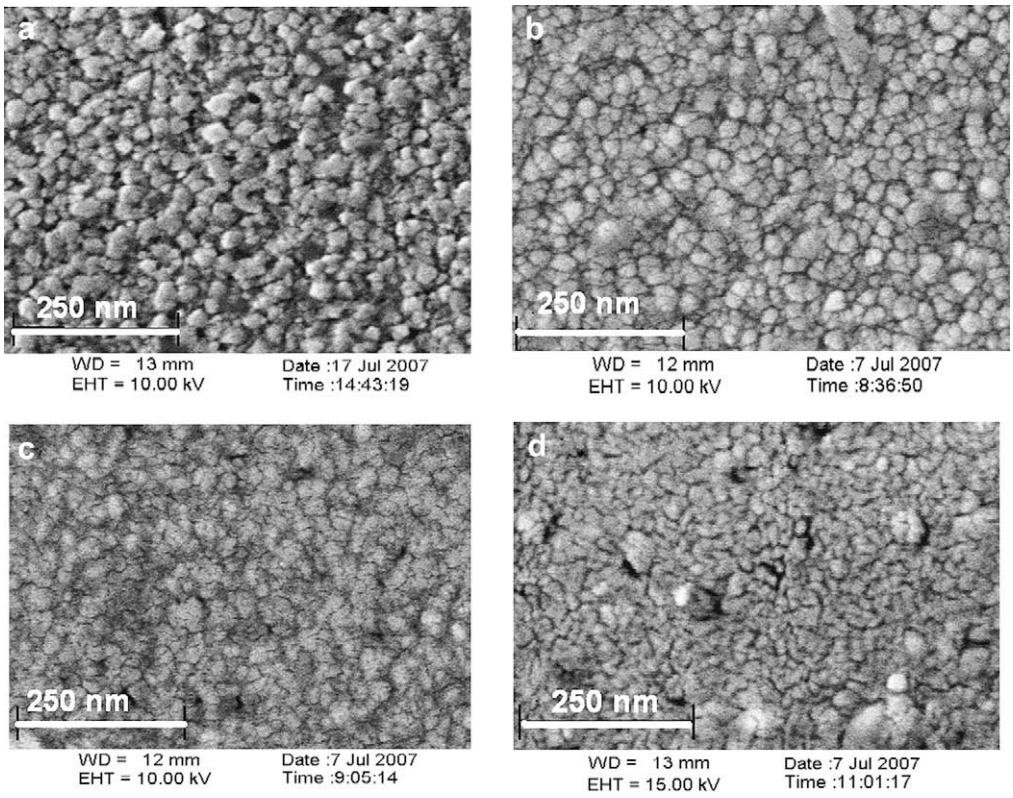

Fig. 3. SEM images of undoped and Fe-doped SnO_2 films: (a) undoped SnO_2 film, (b) SnO_2:Fe (4.0 at%), (c) SnO_2:Fe (7.8 at%), and (d) SnO_2:Fe (39.6 at%).

increasing temperature higher than 350 K. The linear manner in temperatures below 350 K is related to free electron model while large nonlinear variations are related to the electron–phonon and phonon–phonon interactions, which are temperature dependent phenomena [5]. There is a considerable Seebeck coefficient for doping levels of 7.8 at% and 15.7 at% in 350–450 K range. For this region, typical value of Seebeck coefficient varies between +4 and +6 mV/K, which is a considerably large value amongst thin film and bulk thermoelectric materials. In addition, in doping levels less than 7.8 at%, Seebeck coefficient is very low ~−0.2 mV/K to −0.28 mV/K and film shows n-type conductivity, while for doping levels more than 7.8 at% is high and film exhibits p-type conductivity. However, the Seebeck coefficient in doping levels more than 15.7 at% falls to low values due to increasing resistivity and disorders in the film's crystalline structure, in agreement to other reports [5,21]. Fig. 5 displays the variation

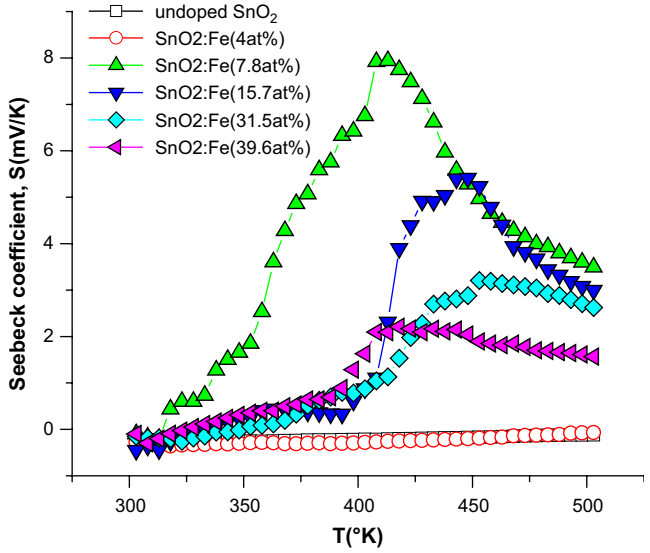

Fig. 4. Seebeck coefficient (S) versus temperature for various Fe-doped SnO_2 films.

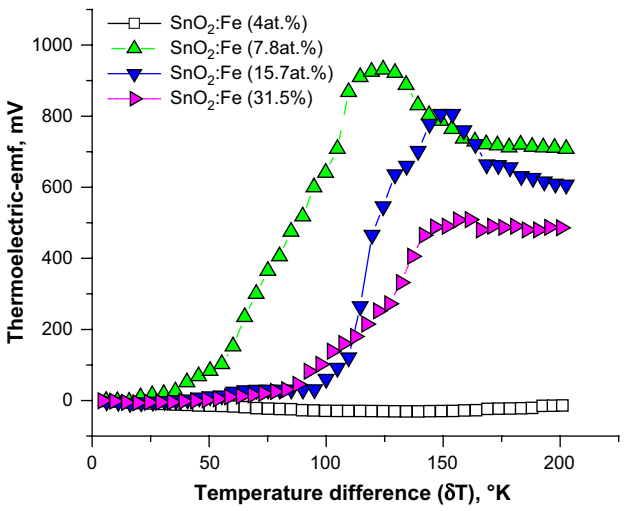

Fig. 5. The variation of thermoelectric e.m.f. with temperature difference (δT) for undoped and Fe-doped SnO_2 films.

of thermoelectric e.m.f. versus temperature difference (δT). It is seen that the thermoelectric e.m.f. exhibits a nonlinear trend especially for temperature differences in the 50–150 K range. The highest thermoelectric e.m.f. was obtained for 7.8 at% Fe-doping to be 930 mV ($\delta T = 125$ K).

It should be noted that ~30% reduction in thermoelectric e.m.f. (in comparison to the values shown in Fig. 5) was observed after repeating the thermoelectrical measurements. This might be related to the alteration of microstructure, reorientation and compensation for oxygen deficiency of the films, which results in adjustment of the stoichiometry and increasing the electrical resistivity [13]. This thermoelectric e.m.f. reduction was observed only one time; subsequent measurements on aged samples did not show any further variations. It worth to be noted that the study of thermoelectrical behavior of the SnO_2:Fe films is highly dependent on their microstructural properties.

3.3. Optical properties

Fe-doping also has influence on optical band gap of the doped SnO_2 films. Referring to Fig. 6 and Table 2, it is seen that by increasing the doping level, energy gap gradually decreases from 3.87 eV to 3.58 eV, which is related to the carrier density reduction, grain size increase and/or multi-phase nature of the films [22]. In fact, variation of band gap due to doping is a result of Moss–Burstein (MB) effect, in which the band gap can be presented as $E_g = E_{go} + \Delta E_{MB}$, where E_{go} is the intrinsic band gap and ΔE_{MB} is the amount of band gap change (a function of electron or hole concentration) [22–25]. The other reason for optical band gap reduction might be due to appearance of the Fe–Sn metallic compounds, as can be seen in XRD analysis results (see Section 3.1).

Fig. 7 shows the optical transmittance of SnO_2:Fe thin films in 400–1100 nm range. As shown, the average transmittance

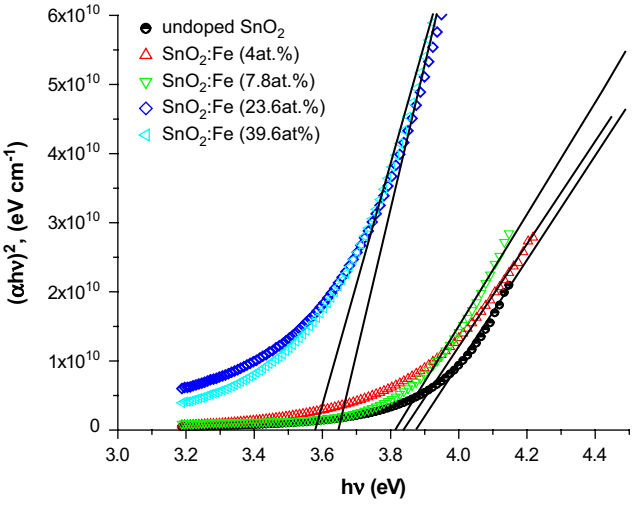

Fig. 6. Plots of $(\alpha h\nu)^2$ versus $h\nu$ (photon energy) for undoped and Fe-doped SnO_2 films. The cross-points of the lines with photon energy ($h\nu$) axis show the value of the E_g.

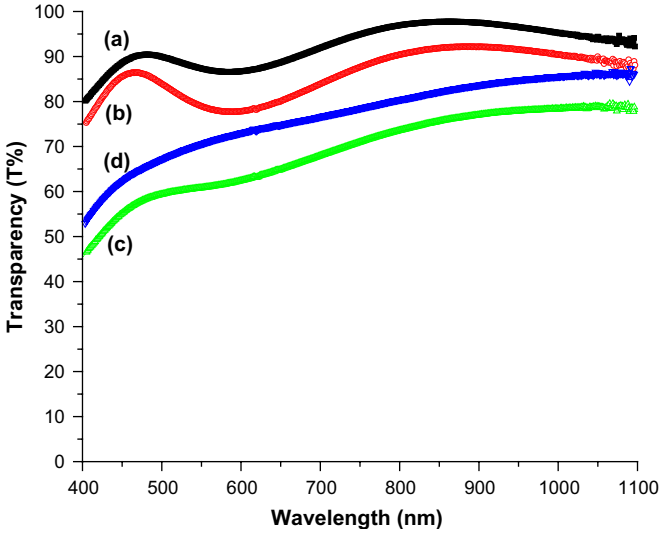

Fig. 7. Optical transparency of various Fe-doped SnO_2 films: (a) 0 at%, (b) 7.8 at%, (c) 23.6 at%, and (d) 39.6 at%.

of the films decreases from ~90% to ~70% when the doping level increases from 0 at% to 23.6 at%, which is related to reduction of crystalline size and escalation of light scattering. However, the average transmittance increases slightly in 39.6 at% doping level.

4. Conclusions

In this paper, we have reported the preparation and characterization of the SnO_2:Fe thin films with high thermoelectric efficiency. These films have been deposited by spray pyrolysis technique. The Hall effect and thermoelectrical measurements have shown p-type conductivity in this films with Fe-doping levels higher than 7.8 at% in precursor solution. Also, the Seebeck coefficient for SnO_2:Fe films with 7.8 at% doping has been obtained to be as high as +1850 μV/K. The XRD and SEM studies of as-deposited samples with thicknesses ~350 nm have shown polycrystalline structure with clear characteristic peak of SnO_2 cassiterite phase. The average optical transparency ($T\%$) of the films in visible spectra decreases from 90% to 75% and electrical resistivity (ρ) increases from 1.2×10^{-2} Ω cm to 3×10^{3} Ω cm with increase of Fe-doping. The electrical, optical and structural characterization results show that SnO_2:Fe transparent conducting films with lower levels of doping exhibit appropriate optical transparency, p-type conductivity along with high thermoelectric efficiency. These films can be utilized as thermoelectric sources and used in transparent p–n junctions.

Acknowledgments

The authors would like to thank Mrs. M. Hassanzadeh from Solid State Physics Research Center, Damghan University of Basic Sciences for XRD analysis and Mrs. M. Houshiar Sadeghian form Central Research Laboratory of Ferdowsi University of Mashhad for SEM analysis.

References

[1] G.S. Nolas, J. Poon, M. Kanatzidis, MRS Bull. 31 (3) (2006) 199.
[2] J.Yang, T. Caillat, MRS Bull. 31 (3) (2006) 224.
[3] Y.G. Gurevich, G.N. Logvinov, Semicond. Sci. Technol. 20 (2005) R57.
[4] Nolas GS, Sharp J, Goldsmid HJ. Thermoelectrics – basic principles and new materials developments. Springer, Berlin; 2001.
[5] H. Imai, Y. Shimakawa, Y. Kubo, Phys. Rev. B 64 (2001) 241104.
[6] K. Koumoto, I. Terasaki, R. Funahashi, MRS Bull. 31 (3) (2006) 206.
[7] A.M. Rao, X. Ji, T.M. Tritt, MRS Bull. 31 (3) (2006) 218.
[8] H. Bottner, G. Chen, R. Venkatasubramanian, MRS Bull. 31 (3) (2006) 211.
[9] S.C. Liufu, L.D. Chen, Q. Yao, C.F. Wang, Appl. Phys. Lett. 90 (2007) 112106.
[10] P. Fournier, X. Jiang, W. Jiang, S.N. Mao, T. Venkatesan, C.J. Lobb, et al., Phys. Rev. B 56 (1997) 14149.
[11] H. Ohta, S. Kim, T. Mizoguchi, K. Nomura, S. Ohta, T. Nomura, et al., Nature Mater. 6 (2007) 129.
[12] R.C. Mallik, V.D. Das, J. Appl. Phys. 98 (2005) 023710.
[13] V.D. Das, K.S. Raju, S. Aruna, J. Appl. Phys. 78 (1995) 1751.
[14] G.U. Sumanasekera, B.K. Pradhan, H.E. Romero, K.W. Adu, P.C. Eklund, Phys. Rev. Lett. 89 (2002) 166802.
[15] T. Mori, T. Nishimura, J Solid State Chem. 179 (2006) 2908.
[16] F. Völklein, V. Baier, U. Dillner, E. Kessler, Thin Solid Films 187 (1990) 253.
[17] H.L. Hartnagel, A.L. Dawar, A.K. Jain, C.J. Jagadish, Semi-conducting transparent thin films, IOP, Bristol, 1995.
[18] Z.Q. Li, J.J. Lin, J. Appl. Phys. 96 (2004) 5918.
[19] T. Ohyama, M. Okamoto, E. Otsuka, J. Phys. Soc. Jpn. 52 (1985) 3571.
[20] M.-M. Bagheri-Mohagheghi, M. Shokooh-Saremi, J. Phys. D Appl. Phys. 37 (2004) 1248.
[21] A.N. Banerjee, R. Maity, P.K. Ghosh, K.K. Chattopadyay, Thin Solid Films 474 (2005) 261.
[22] S.K.F. Ahmed, S. Khan, P.K. Mitra, K.K. Chattopadhyay, J. Sol-Gel Sci. Technol. 39 (2006) 241.
[23] A.I. Martinez, D.R. Acosta, Thin Solid Films 483 (2005) 107.
[24] T. Minami, MRS Bull. 25 (2000) 38.
[25] T.J. Coutts, D.L. Young, X. Li, MRS Bull. 25 (2000) 58.